microstrip patch antenna array with notched band for modern wireless applications. *Microw Opt Technol Lett.* 2015;57:2067–2072.

[25] Singh K, Mulgi SN. Design and development of U-notched corner truncated square microstrip antenna for X to Ku band operation. *Microw Opt Technol Lett.* 2013;55:719–723.

[26] Tahir FA, Naqvi AH. A compact hut-shaped printed antenna for super-wideband applications. *Microw Opt Technol Lett.* 2015;57: 2645–2649.

[27] Tan B-K, Withington S, Yassin G. A compact microstrip-fed planar dual-dipole antenna for broadband applications. *IEEE Antennas Wireless Propag Lett.* 2016;15:593–596.

[28] Zhang H, Mahe Y, Razban T. Low-cost Ku-band dual-polarized and beam switchable cross-type antenna array for satellite communications. *Microw Opt Technol Lett.* 2014;56:2656–2659.

[29] Bhadouria AS, Kumar M. Wide Ku-band microstrip patch antenna using defected patch and ground, in: 2014 Int. Conf. Adv. Eng. Technol. Res. (ICAETR - 2014), IEEE, 2014: 1–5.

[30] Bhowmik LM, Armiento C, Akyurtlu A, Miniscalco W, Chirravuri J, McCarroll C. Design and analysis of conformal ku-band microstrip patch antenna arrays, in: 2013 IEEE Int. Symp. Phased Array Syst. Technol., IEEE, 2013: 815–820.

[31] Ullah MH, Islam MT, Mandeep JS. Printed prototype of a wideband S-shape microstrip patch antenna for Ku/K band applications. *Appl Comput Electromagn Soc J.* 2013;28:307–313.

[32] Ahsan MR, Habib Ullah M, Mansor F, Misran N, Islam T. Analysis of a compact wideband slotted antenna for ku band applications. *Int J Antennas Propag.* 2014;2014:1–6.

[33] Yu C, Hong W, Kuai Z, Wang H. Ku-band linearly polarized omnidirectional planar filtenna. *IEEE Antennas Wireless Propag Lett.* 2012;11:310–313.

[34] Rezaul Azim NM, Tariqul Islam M. Dual polarized microstrip patch antenna for Ku-band application, Inf. MIDEM 41(2011)2, Ljubljana, 2011;41:114–117.

[35] Prasad PC, Chattoraj N. Design of compact Ku band microstrip antenna for satellite communication, in: 2013 Int. Conf. Commun. Signal Process., IEEE, 2013: 196–200.

[36] Islam MM, Islam MT, Faruque MRI. Dual-band operation of a microstrip patch antenna on a duroid 5870 substrate for Ku- and K-bands. *Sci World J.* 2013;2013:1–10.

[37] Ahsan MR, Islam MT, Habib Ullah M, Aldhaheri RW, Sheikh MM. A new design approach for dual-band patch antenna serving Ku/K band satellite communications. *Int J Satell Commun Netw* 2016;34:759–769.

[38] Khandelwal MK, Kanaujia BK, Dwari S, Kumar S. Design and analysis of microstrip DGS patch antenna with enhanced bandwidth for Ku Band applications, in: 2013 Int. Conf. Microw. Photonics, IEEE, 2013: 1–4.

How to cite this article: Mishra B, Singh V, Singh RK, Singh N, Singh R. A compact UWB patch antenna with defected ground for Ku/K band applications. *Microw Opt Technol Lett*. 2017;60:1–6. https://doi.org/10.1002/mop.30911

Received: 4 June 2017

DOI: 10.1002/mop.30915

Semi-transparent frequency reconfigurable antenna with DGS

M.C. Lim[1] | S.K.A. Rahim[1] | M.R. Hamid[2] | P.J. Soh[3] | Aa Eteng[4]

[1] Wireless Communication Centre (WCC), Universiti Teknologi Malaysia, Johor Bharu, Johor 81310, Malaysia

[2] Radio Communications Engineering, Universiti Teknologi Malaysia, Faculty of Electrical Engineering, Skudai, Johor, Malaysia

[3] Advanced Communications Engineering (CoE), School of Computer and Communication Engineering, Universiti Malaysia Perlis, Arau, Perlis 02600, Malaysia

[4] Department of Electronic and Computer Engineering, Faculty of Engineering University of Port Harcourt, Port Harcourt, Nigeria

Correspondence
S.K.A. Rahim, Wireless Communication Centre (WCC), Universiti Teknologi Malaysia, Johor Bharu, Johor 81310, Malaysia.
Email: sharulkamal@fke.utm.my

Abstract

In this letter, a semi-transparent frequency reconfigurable antenna is proposed and investigated. This antenna is implemented on glass as a substrate, AgHT-4 as a radiating element and copper as its ground plane to result in a semi-transparent feature. A pair of PIN diodes is utilized as microwave switches along with a DC biasing circuit. This proposed antenna is fed by a CPW arrangement and introduces unequal E-shaped Defected Ground Structure (DGS) on the ground plane for modification of the electrical length. The antenna exhibits a −10 dB impedance bandwidth from 3 to 6 GHz when PIN diodes are ON, and a resonance at 4.75 GHz when pin diodes are OFF. The proposed antenna is fabricated to validate its performance in terms of reflection coefficient and radiation pattern.

KEYWORDS

CPW, frequency reconfigurable antenna, narrowband, transparent antenna, wideband

1 | INTRODUCTION

Because of the demand for wireless technologies, antenna designs have been intensively researched to cater to size

TABLE 1 Parameters of the proposed frequency reconfigurable antenna

Parameter	Dimensions (mm)	Parameter	Dimensions (mm)
W_s	51	L_{g1}	15.2
W_g	37	L_{g2}	14.6
W_{g1}	16.35	L_c	5
W_{g2}	6	L_f	16.2
W_c	14	P_x	14.5
W_f	3.5	P_y	8.8
L_s	39.3	g	0.4

reduction for compactness, multiwireless functionality, and enhanced performance using emerging materials. The use of frequency reconfigurable antenna on a single hardware is an efficient alternative which ensures space efficiency on compact mobile devices. Recently, transparent antennas have been receiving considerable research attention due to aesthetic reasons, such as when integrating such components on the external section of mobile devices or when solar-energy harvesting components are placed beneath such structures. Currently, most existing antennas are fabricated on opaque microwave substrates such as FR4, Taconic and RT-Duroid due to their well-known behavior. However, these materials are unsuitable for use externally in applications which need transparency.

Various types of transparent conductive films (TCF) have been reportedly used in antenna applications such as indium tin oxide (ITO), fluorine-doped tin oxide (FTO), silver coated polyester film (AgHT), and silver grid layer (AgGL) and silver nano wire (AgNw). These materials differ in thickness, transmittance and sheet resistance. ITO has a transmittance of 85%. However, its sheet resistance (R_s) is low, ~15 Ω sq^{-1}, with mid-temperature process in 200°C. Meanwhile, TCF is considered unsuitable for antennas due to its high sheet resistance, a major factor which limits the use of transparent antennas.[1] Commercial AgHT can be categorized into two types, namely AgHT-4 and AgHT-8. In terms of visible transmittance, AgHT-4 TCF exhibits 75% and Rs of at least 4.5 ± 1 Ω sq^{-1}, whereas AgHT-8 has a higher visible transmittance of 82%, with a higher sheet resistance of 8 ± 1 Ω sq^{-1} (±1Ω).[2]

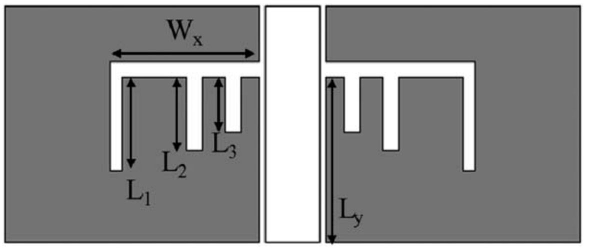

FIGURE 2 Geometry of the *E*-shaped DGS

Over the past decade, UWB,[3–5] band-notched,[6] circularly polarized[7] and dual-band antennas[8] antennas using transparent materials have been proposed. The antenna in Ref. [3] covers an impedance bandwidth from 500 MHz to 10.6 GHz, and is implemented using AgHT-8 as a patch on a 1-mm-thick glass substrate and ITO as a ground plane. It is fed using a microstrip transmission line. Meanwhile, another highly transparent antenna made using AgHT-8 as the radiating element and PET as a substrate is proposed in Ref. [5] to reduce its weight. The proposed antenna is implemented

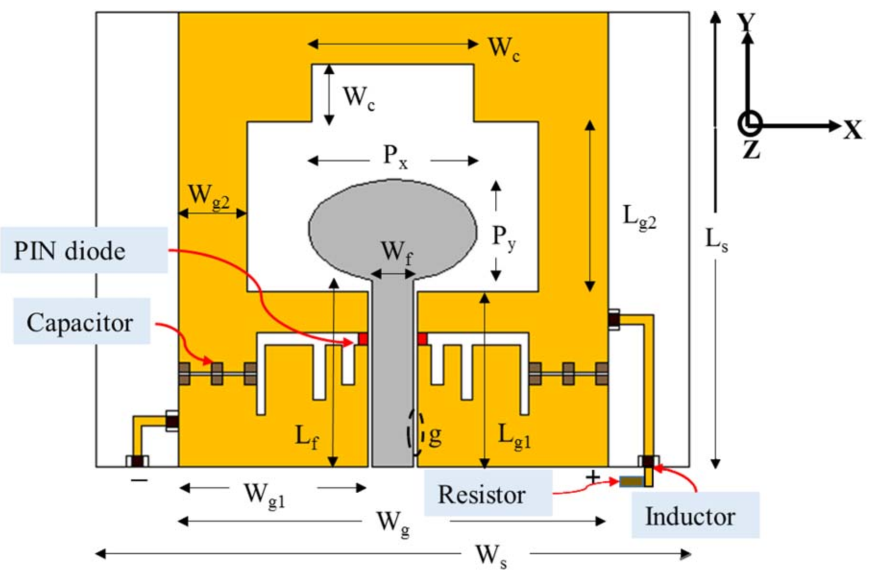

FIGURE 1 Geometry and DC biasing circuit of the proposed antenna. [Color figure can be viewed at wileyonlinelibrary.com]

TABLE 2 Optimized parameters of the *E*-shape DGS

Parameters	L_1	L_2	L_3	W_x
Dimensions (mm)	6	4.7	3.5	9.5

using a staircase technique to increase the overlap of resonant frequencies, besides using two symmetrical rectangular stubs to increase the bandwidth between 3.15 and 32 GHz. Next, a band-notched UWB antenna at 5.8 GHz was proposed in Ref. [6]. This antenna is constructed using transparent AgHT-4 thin film and integrates a complementary split-ring resonator (CSRR) to create a stop band within the 5.8 GHz ISM band. Besides that, a circularly-polarized transparent antenna operating in the 5.8 GHz for WLAN applications was proposed in Ref. [7]. This antenna was fabricated using AgHT-4 as the radiating element. The tapered split gap and inequality in the lengths of the CPW ground arms contributed to a wide 3 dB axial ratio bandwidth from 5.4 to 6.2 GHz.

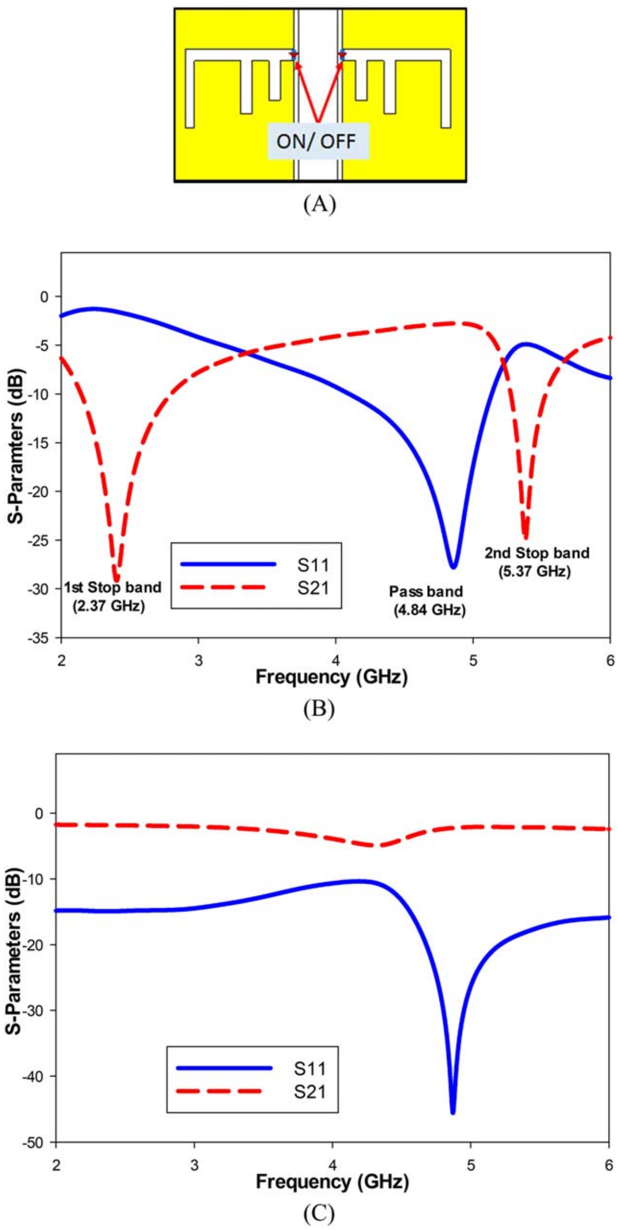

FIGURE 3 (A) Location of the switches; (B) bandpass response; and (C) bandstop response. [Color figure can be viewed at wileyonlinelibrary.com]

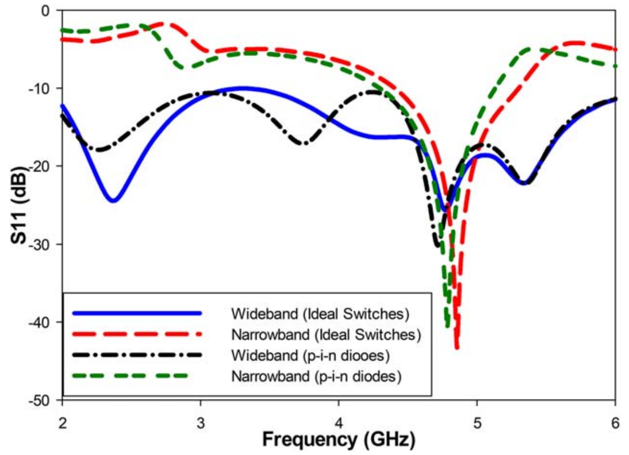

FIGURE 4 Comparison of simulated reflection coefficient (S_{11}) between the use of copper pads and PIN diodes. [Color figure can be viewed at wileyonlinelibrary.com]

Defected ground structures (DGS) typically suppress surface waves and provides arbitrary stopbands[9] by modifying the current distribution on the ground plane. Therefore, it changes the line capacitance and inductance, while also functioning as a prefiltering circuit.[10] Numerous of works have reported the integration of DGS into antenna to achieve frequency reconfigurability. For instance, a wideband-to-narrowband reconfiguration was investigated in Refs. [11] and [12]. The narrowband operations can be switched from a wideband behavior by employing multiple PIN diodes along a pair of ring slots to change their electrical lengths. Another investigation in Ref. [13] presented DGS meandered slot lines on the ground plane of a CPW-fed antenna to enable wideband-to-narrowband reconfigurability. The lengths of meandered slot functions as a filter to tune the resonant frequency.

In this letter, a semitransparent frequency reconfigurable antenna featuring wideband and narrowband reconfigurability is presented. To the authors' best knowledge, this is the first TCF-based frequency reconfigurable antenna reported in literature. A pair of unequal E-Shaped DGS is integrated on the ground plane to enable narrowband operation centered at 4.75 GHz for radar application. Its operation can be switched to wideband mode (from 2 to 6 GHz) by eliminating the functionality of the DGS resonator when PIN diodes are turned ON. The use of AgHT-4, copper foil and glass in the proposed antenna design enables its semitransparent feature, which may be suited for future solar energy harvesting feature in compact devices.

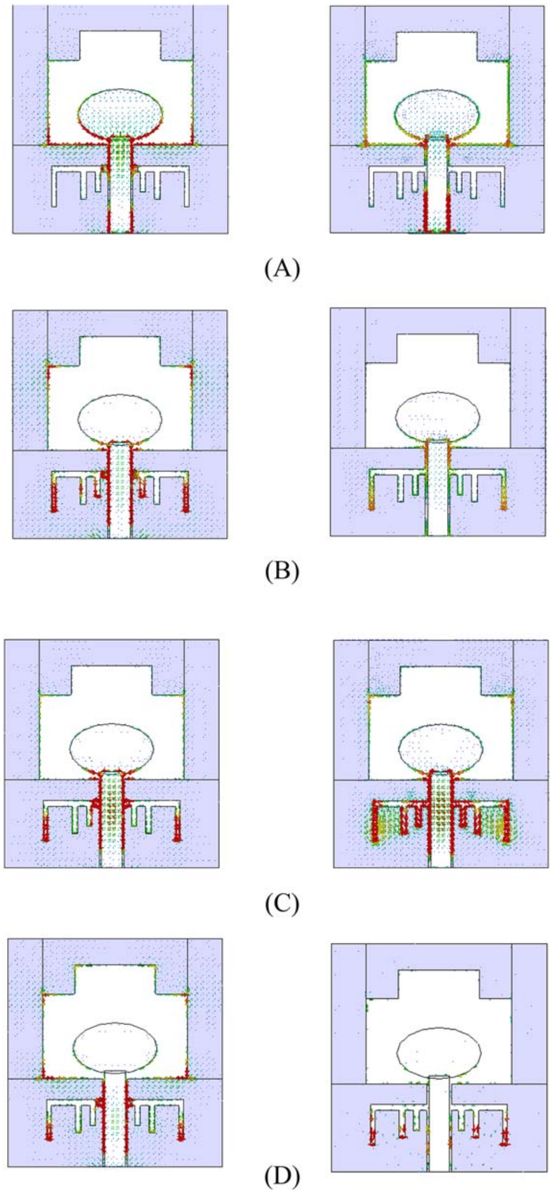

FIGURE 5 Simulated surface current distribution for the wideband mode (left) and narrowband (right) mode at: (A) 3 GHz (B) 4 GHz (C) 4.75 GHz (D) 5.5 GHz. [Color figure can be viewed at wileyonlinelibrary.com]

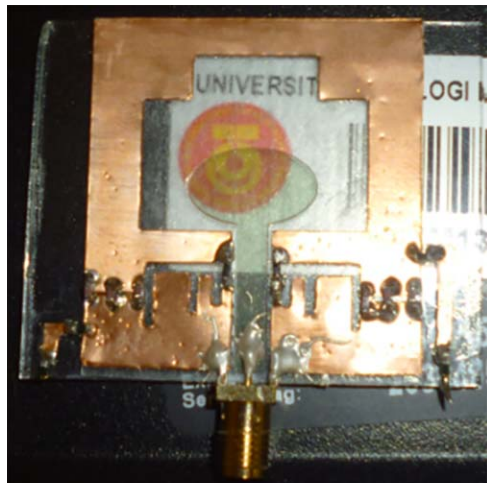

FIGURE 6 Photograph of the fabricated semi-transparent frequency reconfigurable antenna. [Color figure can be viewed at wileyonlinelibrary.com]

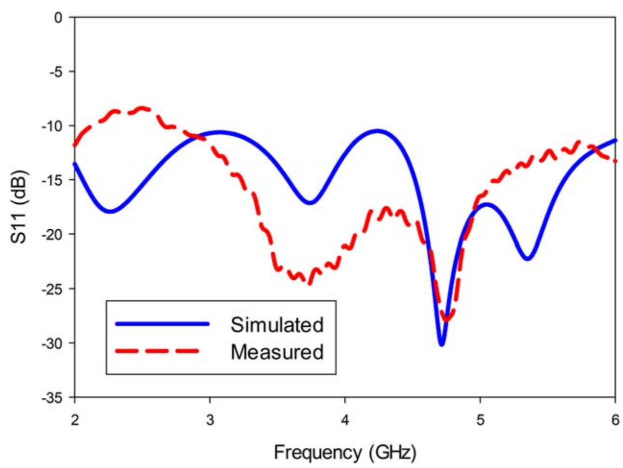

FIGURE 7 Simulated and measured reflection coefficient (S_{11}) for the wideband mode. [Color figure can be viewed at wileyonlinelibrary.com]

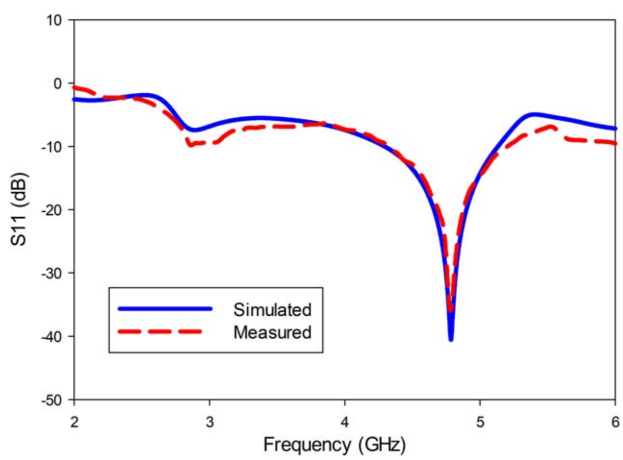

FIGURE 8 Simulated and measured reflection coefficient (S_{11}) for the narrowband mode. [Color figure can be viewed at wileyonlinelibrary.com]

2 | ANTENNA DESIGN

This antenna is inspired by the design in Ref. [14], with the E-shaped DGS added enable reconfiguration to the narrowband mode centered at 4.75 GHz. This structure comprises of an AgHT-4 layer and copper foil as the conductive elements, and an optical glass substrate, with a relative permittivity (ε_r) of 6.07 and thickness (t) of 2 mm. The AgHT-4 structure consists of two main parts: the silver conductive layer and polyethylene terephthalate (PET). It features $R_s = 4$ Ω sq^{-1} and $\varepsilon_r = 3.228$ and thicknesses of 0.0525 and 0.1225 mm. Both AgHT-4 and glass are transparent, while

TABLE 3 Summary of the antenna performance

Switches state	Mode	Bandwidth (simulated)	Bandwidth (measured)	Gain (simulated)
ON-ON	Wideband	2–6 GHz (100%)	2–6 GHz (100%)	1.66 dBi (Peak Gain at 5.5 GHz)
OFF-OFF	Narrowband	4.34–5.1 GHz (16%)	4.33–5.2 GHz (18%)	1.433 dBi (at 4.75 GHz)

the copper foil serves as the antenna ground plane. Besides that, a DC biasing circuit comprising of inductors and capacitors are added to operate the PIN diodes. Finally, a DGS pre-filtering circuit is implemented on the ground-plane. The total size of the proposed antenna is only 51 mm × 39.3 mm, including the additional 7 mm on each side of the antenna to place the biasing traces of the DC circuit. The optimized geometrical parameters of the structure are summarized in Table 1.

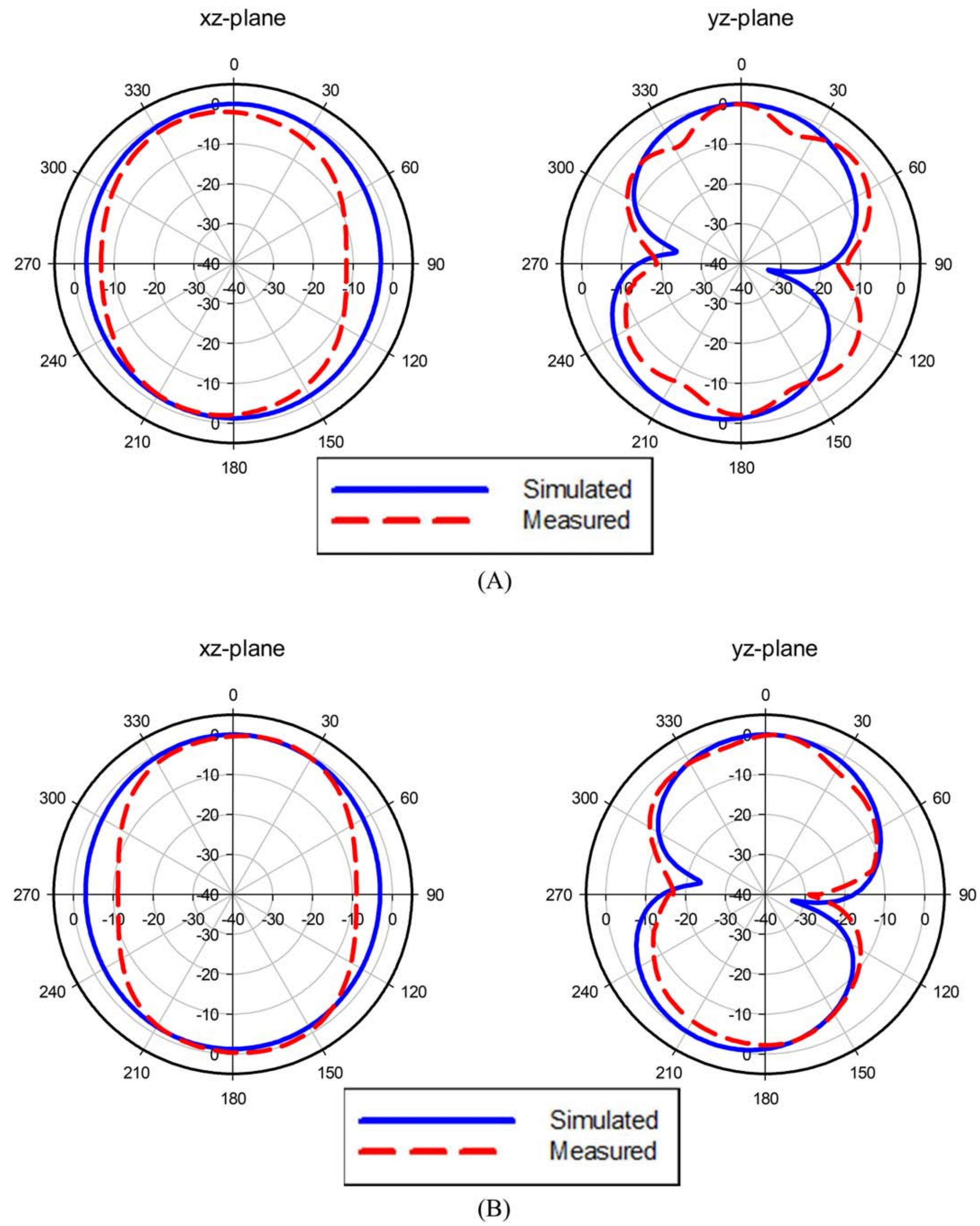

FIGURE 9 Simulated and measured radiation patterns for the wideband mode (Left *xz* plane; Right *yz* plane) at: (A) 3 GHz (B) 4 GHz (C) 4.75 GHz (D) 5.5 GHz. [Color figure can be viewed at wileyonlinelibrary.com]

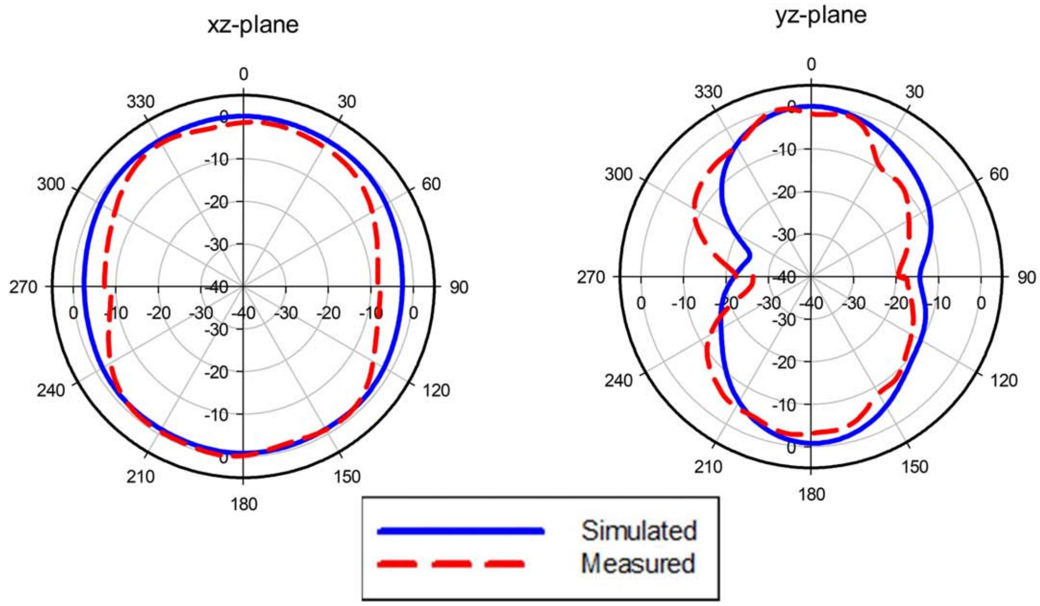

(C)

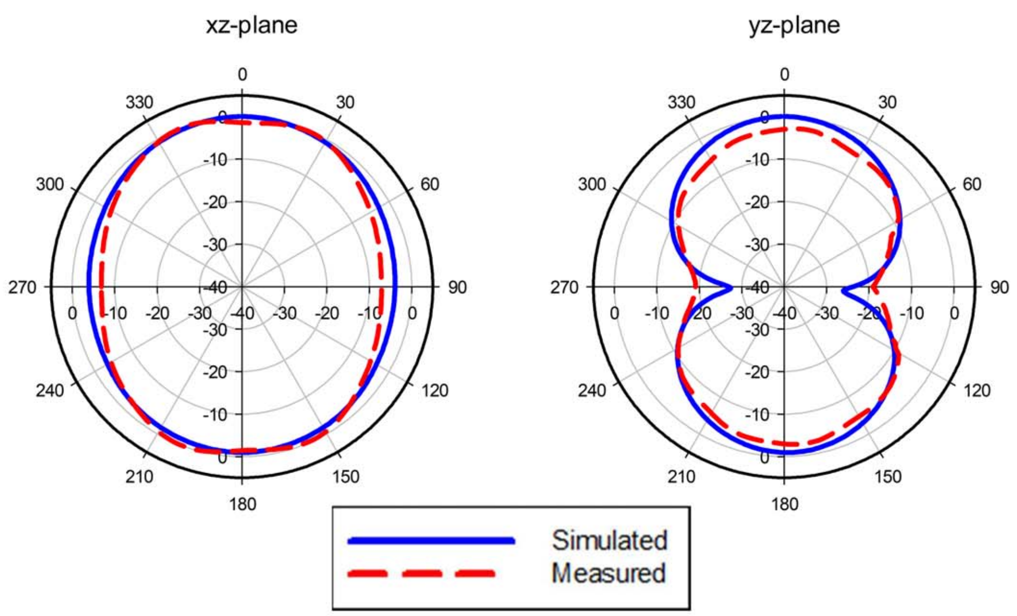

(D)

FIGURE 9 Continued

The geometry and DC biasing circuit of proposed semi-transparent frequency reconfigurable antenna is depicted in Figure 1. Each side of the ground plane is allocated a PIN diode at an end point of the slot, acting as ON/OFF switches for current flow control. A two-terminal supply (positive on the left and negative on the right) is also added for the DC power supply. A 100 Ω film resistor is connected to the positive supply as a load to prevent a short circuit. In the DC biasing circuit, 3-mm slits are etched on the ground plane to isolate DC bias supply. Capacitors are placed on the slits to isolate DC power, while allowing the RF wave signal to flow through them. Besides that, a 100 pH inductor is connected in series on the DC bias line to function as an RF choke, creating high impedance and preventing RF signal flow into the DC bias line.

To obtain narrowband reconfigurability, a pair of horizontal *E*-shaped DGS slot lines are integrated on the CPW ground-plane as a filtering circuit (see Figure 2). The center frequency of this narrowband mode can be controlled by adjusting the perimeter of the slots, with its lengths denoted as W_X, L_1, L_2, and L_3. The total perimeter of these slots is approximately a quarter-wavelength (λ/4) at the center frequency of this narrowband mode. The optimization of L_y is to improve the reflection coefficient for the narrowband

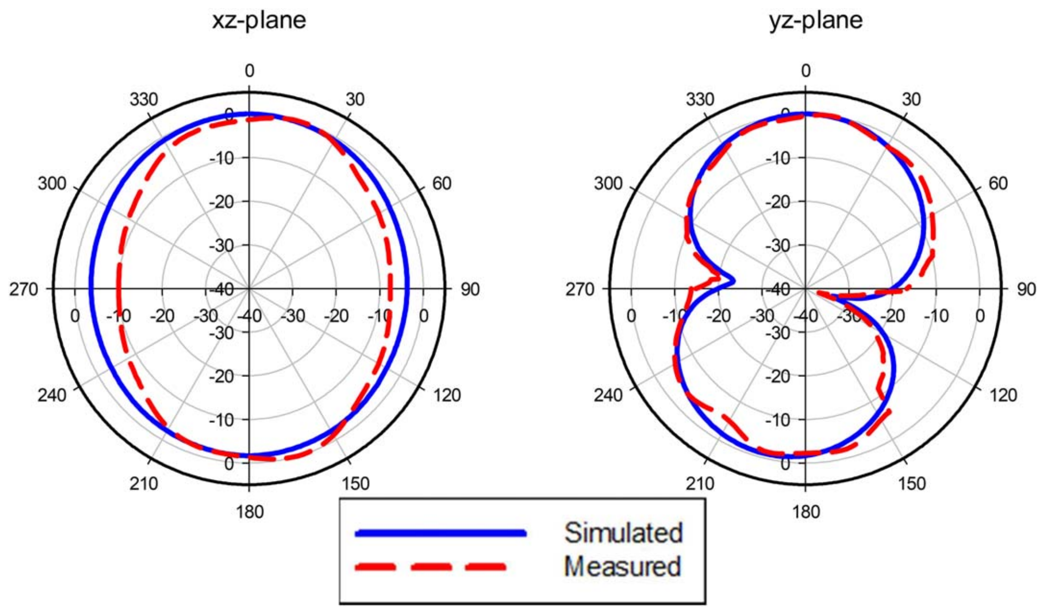

FIGURE 10 Simulated and measured radiation patterns for the narrowband mode (Left *xz* plane; Right *yz* plane) at 4.75 GHz. [Color figure can be viewed at wileyonlinelibrary.com]

mode, whereas the other optimized parameters of the slot lines are summarized in Table 2. Figure 3A depicts the geometry of the DGS with PIN diodes, while Figure 3B,C presents the S-parameters (reflection coefficient and insertion loss) for both the wideband- and narrowband reconfigurations. When the PIN diode is in the OFF state, the *E*-shaped DGS acts as a bandpass filter, generating two stopbands (2.37 and 5.37 GHz) and one passband (4.84 GHz) as shown in Figure 3B. To switch to a wideband mode, PIN diodes need to be ON, activating the bandstop filter. Hence, the DGS is eliminated to enable the antenna to maintain its wideband mode, see Figure 3C.

3 | RESULTS AND DISCUSSION

As an initial validation, the simulated and measured reflection coefficients using ideal switches and copper pads are compared in Figure 4. The use of the ideal switch indicated a slight upwards frequency shift for the narrowband mode by 0.05 GHz due to a neglect of parasitic effects in the simulations. Meanwhile, the reflection coefficient did not change significantly in the wideband operating mode when using copper pads to emulate PIN diodes, with similar −10 dB bandwidth. It can be concluded that the ideal switches are representative of the real switches and is suitable for use in the initial design phase to simplify the optimization process and reduce simulation time.

The surface current distribution of the structure is further studied as illustrated in Figure 5, using copper pads to ease the visualization. They are divided into the ON and OFF states at the frequencies of 3, 4, 4.75, and 5.5 GHz. During the ON state, an ideal switch is placed at the end point of each ground plane. It is observed that a high current distribution density is concentrated in the region which disabled the *E*-shaped resonator functionality, resulting in a wideband operation. Upon removing the copper pads from the groundplane, the *E*-shaped DGS is operational, triggering the narrowband mode. As shown in Figure 5A, B, and D, the current distributions for the OFF state at 3, 4, and 5.5 GHz are very weak on the slot, due to its function as a selective stop band filter. The strongest surface current density occurring at 4.75 GHz indicates the resonance of the *E*-shaped DGS at this particular frequency.

The optimized antenna is then prototyped, as illustrated in Figure 6 for measurement purposes. Figure 7 shows the simulated and measured reflection coefficient of the wideband mode, which is triggered by turning ON both PIN diodes and eliminating the functionality of the DGS. This consequently activates the bandstop filter characteristic. Simulations indicated that the wideband mode operates with a −10 dB bandwidth over the entire 2–6 GHz. However, measurements indicate a slight degradation at the upper frequency, which is slightly above −10 dB. This is due to fabrication errors and the resistivity variation of the semitransparent material.

Having both PIN diodes in the OFF state activates the *E*-shaped DGS bandpass filter to suppress unwanted frequencies and allow a passband centered at 4.75 GHz. The comparison between simulated and measured reflection coefficient in Figure 8 indicates a good agreement. The narrowband mode is validated to be operating from 4.34 to 5.1 GHz with a 1.433 dBi gain, and is suited for indoor radars and cognitive radio applications.[15] Meanwhile, the peak gain throughout the wideband mode is 1.66 dBi. This is due to the lossy FR4 substrate and limited conductivity of AgHT-4. A summary of the antenna performance is provided in Table 3.

Figure 9 illustrates the simulated and measured wideband mode radiation patterns in the *xz*-plane (left) and *yz*-plane (right) at four different frequencies: 3, 4, 4.75, and 5.5 GHz. Meanwhile, Figure 10 illustrates the radiation pattern for the narrowband mode (when the PIN diodes are in the OFF state) at 4.75 GHz. The antenna exhibits a quasi-omnidirectional pattern in the *xz*-plane and is bidirectional in the *yz*-plane. A good agreement is observed between simulations and measurements.

4 | CONCLUSION

A semitransparent frequency reconfigurable antenna has been designed and investigated. The antenna is first optimized for a wide bandwidth operation from 2 to 6 GHz. Next, the *E*-shaped DGS is introduced on the CPW ground plane to enable its reconfiguration into to a narrowband mode centred at 4.75 GHz. A pair of PIN diodes is placed at two ends of the DGS to enable the narrowband mode when the PIN diodes are in the OFF state, with a fractional bandwidth of 16%. On the other hand, a wideband operation with 100% fractional bandwidth is enabled when the PIN diodes are in the ON state. Assessment results indicated good agreements between simulations and measurements, with quasi-omnidirectional patterns in the *xz*-plane and bidirectional radiation in the *yz*-plane.

ORCID

M.C. Lim http://orcid.org/0000-0001-9618-1747

REFERENCES

[1] Li QL, Cheung SW, Wu D, Yuk TI. Optically transparent dual-band MIMO antenna using micro-metal mesh conductive film for WLAN system. *IEEE Antennas Wireless Propagat Lett.* 2017;16:920–923.

[2] Gredmann. 2004. AgHT^{TM} Product Line, CPFilms. Inc, Retrieved October 28, 2013. Available at: www.cpfilms.com

[3] Peter T, SWC, Rahim SKA, Tharek AR. "Grounded CPW Transparent UWB Antenna for UHF and Microwave Frequency Application," Progress in Electromagnetics Research Symposium Proceedings, Taipei, Taiwan, pp. 479–481, 2013.

[4] Peter T, Cheung RN. "A Novel Transparent TSA for Laptop and UWB Applications," Paper presented at the PIERS Proceedings, Kuala Lumpur, Malaysia, pp. 836–838, 2012.

[5] Hakimi S, Rahim SKA, Abedian M, Noghabaei SM, Khalily M. CPW-fed transparent antenna for extended ultrawideband applications. *IEEE Antennas Wireless Propagat Lett.* 2014;13:1251–1254.

[6] Rani MSA, Rahim SKA, Kamarudin MR, Peter T, Cheung SW, Saad BM. Electromagnetic behaviors of thin film CPW-fed CSRR loaded on UWB transparent antenna. *IEEE Antennas Wireless Propagat Lett.* 2014;13:1239–1242.

[7] Wahid WIMRK, Khalily M, Peter T. Circular polarized transparent antenna for 5.8 GHz WLAN applications. *Prog Electromagn Res Lett.* 2015;57:39–45.

[8] Malek MA, Hakimi S, Abdul Rahim SK, Evizal AK. Dual-band CPW-fed transparent antenna for active RFID tags. *IEEE Antennas Wireless Propagat Lett.* 2015;14:919–922.

[9] El-Shaarawy HB, Coccetti F, Plana R, El-Said M, Hashish EA. Novel reconfigurable defected ground structure resonator on coplanar waveguide. *IEEE Trans Antennas Propagat.* 2010;58:3622–3628.

[10] Weng LH, Guo YC, Shi XW, Chen XQ. An overview on defected ground structure. *Prog Electromagn Res B.* 2008;7:173–189.

[11] Hamid MR, Gardner P, Hall PS, Ghanem F. Vivaldi antenna with integrated switchable band pass resonator. *IEEE Trans Antennas Propagat.* 2011;59:4008–4015.

[12] Tariq A, Hamid MR, Ghafouri-Shiraz H. "Reconfigurable monopole antennas," Proceedings of the 5th European Conference on Antennas and Propagation (EUCAP), pp. 2160–2164, 2011.

[13] Dahalan FD, Rahim SKA, Hamid MR, et al. Frequency-reconfigurable Archimedean spiral antenna. *IEEE Antennas Wireless Propagat Lett.* 2013;12:1504–1507.,

[14] Lim MC, Rahim SKA, Hamid MR, Eteng AA, Jamlos MF. Frequency reconfigurable antenna for WLAN application. *Microwave Opt Technol Lett.* 2017;59(1):171–176.

[15] Nabilah Ripin NFG, Asari Sulaiman A, Abd Rashid NE, Fahmi Hussin M. Size miniaturization and bandwidth enhancement in microstrip antenna on a couple circular ring DGS. *Int J Latest Res Sci Technol.* 2015;4(4):27–30.

How to cite this article: Lim MC, Rahim SKA, Hamid MR, Soh PJ, Eteng A. Semi-transparent frequency reconfigurable antenna with DGS. *Microw Opt Technol Lett*. 2017;60:6–13. https://doi.org/10.1002/mop.30915

Received: 10 June 2017

DOI: 10.1002/mop.30914

Gigabit LED-based visible light transparent transmission from free-space to a 100-m ultra-large effective area pure silica fiber

Jianyang Shi[1] | **Yingjun Zhou**[1] | **Nan Chi**[1] | **Liangming Xiong**[2] | **Jie Luo**[2]

[1] Key Laboratory for Information Science of Electromagnetic Waves (MoE), Department of Communication Science and Engineering, Fudan University, Shanghai 200433, China

[2] State Key Laboratory of Optical Fibre and Cable Manufacture Technology, Yangtze Optical Fibre and Cable Company Ltd, Wuhan 430073, China